International Journal of Nanomedicine

Dovepress
Taylor & Francis Group

Open Access Full Text Article

ORIGINAL RESEARCH

Royal Jelly-Derived Extracellular Vesicles: Key Bioactive Components Mediating Anti-Hepatocellular Carcinoma Activity

Xuepeng Chi[1–3], Lingyu Jia[1–3], Ying Wang[1–3], Chao Liu[4], Shuai Wang[5], Zhenguo Liu[1–3], Ge Zhang[1–3], Baohua Xu[1–3]

[1]Key Laboratory of Efficient Utilization of Non-Grain Feed Resources (Co-Construction by Ministry and Province), Shandong Agricultural University, Tai'an, Shandong, People's Republic of China; [2]Shandong Provincial Key Laboratory of Animal Nutrition and Efficient Feeding, Shandong Agricultural University, Tai'an, Shandong, People's Republic of China; [3]Department of Animal Science, Shandong Agricultural University, Tai'an, Shandong, People's Republic of China; [4]Department of Minimally Invasive Oncology, Tai'an City Central Hospital, Tai'an, Shandong, People's Republic of China; [5]Beekeeping Division, Shandong Provincial Animal Husbandry and Veterinary Bureau, Ji'nan, Shandong, People's Republic of China

Correspondence: Baohua Xu, Department of Animal Science, Shandong Agricultural University, Tai'an, Shandong, 271017, People's Republic of China, Email bhxu@sdau.edu.cn

Purpose: To investigate the role of royal jelly derived extracellular vesicles (RJEVs) as key active components contributing to the anti-hepatocellular carcinoma (HCC) effects of royal jelly and to elucidate the underlying mechanisms.

Patients and Methods: This study used H22 tumor-bearing mice as an in vivo model. RJEVs were isolated and identified and their effects were evaluated after oral administration. Analyses included the assessment of liver-targeting properties, immune and antioxidant responses, gut microbiota composition (specifically Muribaculaceae abundance), and short-chain fatty acid metabolism. This study also examined the influence of RJEVs on translation-related signaling networks and the Phosphatidylinositol 3-kinase (PI3K) / Protein Kinase B (AKT) signaling pathway to determine their role in promoting tumor cell apoptosis.

Results: Orally administered RJEVs exhibited liver-accumulating properties in H22 tumor-bearing mice and demonstrated moderate antitumor efficacy. They enhanced immune and antioxidant responses, increased the abundance of Muribaculaceae, modulated gut microbiota composition, and improved short-chain fatty acid metabolism. Mechanistically, RJEVs synergistically regulate translation-related signaling networks and remodel the immune microenvironment, ultimately promoting tumor cell apoptosis via the PI3K/AKT signaling pathway.

Conclusion: These findings provide novel insights into the functional role of royal jelly by identifying RJEVs as important bioactive constituents that contribute to the anti-HCC effects by modulating the immune microenvironment, gut microbiota, and PI3K/AKT signaling. This offers both theoretical and methodological advances in research on the bioactive components of bee products.

Keywords: PI3K/AKT signaling pathway, gut microbiota, apoptosis, immunomodulation, antioxidant

Introduction

The therapeutic potential of bee-derived products and other natural compounds is increasingly recognized in modern healthcare, with growing evidence supporting their pharmacological efficacy across diverse conditions.[1] Among these, royal jelly (RJ) —a secretion from the hypopharyngeal and mandibular glands of nurse honeybees (Apis mellifera)—known for its rich biochemical composition and broad pharmacological properties. RJ contains proteins, carbohydrates, lipids, vitamins, minerals, flavonoids, polyphenols, and multiple biologically active compounds.[2] As the sole nutritional source for larvae and the adult queen, RJ underpins the queen's unique physiological traits, including larger body size, enhanced fertility, and extended lifespan compared to worker bees.[3,4]

Beyond its role in sustaining honeybee biology, emerging evidence demonstrates that RJ exerts pleiotropic health benefits in mammals, including antineoplastic, immunomodulatory, and metabolic regulatory effects, though the underlying molecular mechanisms remain incompletely understood.[5] Our previous work revealed that RJ and selenium-enriched RJ suppress hepatocellular carcinoma (HCC) progression by concurrently modulating PI3K/AKT survival signaling and VEGF-mediated

https://doi.org/10.2147/IJN.S609268
Received: 14 March 2026
Accepted: 22 May 2026
Published: 3 June 2026

angiogenesis.[6] However, those studies treated RJ as a complex whole substance, and the specific constituents responsible for its antitumor activity remained unidentified.

Exosome-like nanoparticles (ENs), also referred to as extracellular vesicles (EVs), have emerged as key mediators of intercellular communication through the transfer of proteins, nucleic acids, and bioactive lipids.[7,8] Historically, research has centered on EVs from bodily fluids, particularly for diagnostic applications.[9] More recently, food-derived EVs or ENs in various dietary sources, including bovine colostrum, plant exudates, and apicultural products, have demonstrated tissue-targeting capabilities and therapeutic potential.[10–13] These dietary ENs are absorbed through the intestine, exert local effects, and reach distant organs via systemic circulation. Notably, food-derived ENs are biocompatible, biodegradable, and non-toxic, without adverse effects on intestinal barrier integrity or other organs.[13] Their ability to regulate physiological and pathological processes underscores their potential as safe natural therapeutic carriers.[10] Given the growing recognition that food-derived extracellular vesicles can mediate inter-kingdom communication and exert therapeutic effects, we hypothesized that RJ-derived EVs (RJEVs) may represent a key bioactive fraction contributing to the anti-HCC activity of RJ.

HCC remains one of the most prevalent malignancies worldwide, with high incidence and mortality.[14] Current multimodal treatments—combining surgical resection with adjuvant chemoradiation—offer only modest survival improvements and are associated with severe off-target toxicities, including myelosuppression, cardiotoxicity, and secondary cancers.[15,16] These limitations have driven interest in nutraceutical interventions, particularly food-derived bioactive compounds with selective antitumor activity.[17–19] Recent studies show that plant- and food-derived ENs, such as those from black mulberry, ginger, and asparagus, possess therapeutic efficacy in liver diseases, highlighting their potential application in HCC therapy.[20]

In bee products, EVs present in pollen, honey, and RJ contribute significantly to their antibacterial and pro-regenerative effects.[21,22] Based on these findings and our previous work demonstrating the anti-HCC activity of crude RJ, we hypothesized that RJEVs contribute significantly to the antitumor efficacy of RJ. In this study, we isolated and characterized RJEVs and evaluated their anti-HCC activity. We demonstrated that RJEVs induce tumor cell apoptosis through inhibition of the PI3K/AKT pathway both in vitro and in vivo. The primary goal of this work was to establish RJEVs as functionally important bioactive constituents of RJ and to elucidate their mechanisms of action. And the liver-accumulating properties of RJEVs observed in our biodistribution studies also suggest their potential as a natural nanoplatform for future development of HCC-targeted drug delivery systems, although this application remains to be experimentally investigated. Material and methods.

Preparation of RJ

RJ was harvested from 10 healthy sister bee colonies at the Shandong Agricultural University experimental apiary (36.16° N, 117.16° E) following our previously described protocol and stored at −20 °C until use.[6]

Isolation of RJEVs

Based on the characteristics of RJ, we slightly modified the method for separating RJEVs, based on the separation of honey, RJ, and grapefruit vesicle-like nanoparticles (Figure 1A).[12,21,22] Briefly, 1.5 g RJ was diluted to 10 mL with cold PBS and homogenized by vortexing. The suspension was sequentially centrifuged at 1000 × g for 20 min, 3000 × g for 20 min, and 12,000 × g for 1 h at 4 °C. The resulting supernatant was ultracentrifuged at 70,000 × g for 1 h at 4 °C and filtration through 0.8 μm, 0.45 μm, and 0.22 μm filter membranes. The filtrate was ultracentrifuged at 130,000 g for 1.5 h at 4 °C. The pelleted nanoparticles were washed with PBS, re-ultracentrifuged (130,000 × g, 1.5 h, 4 °C), resuspended in 500 μL PBS, and stored at − 80 °C until further use. The final protein concentration of the RJEV suspension was determined using a BCA Protein Assay Kit (CoWinBioscience, Jiangsu, China). All isolation procedures were performed under sterile conditions to prevent microbial contamination.

Characterization Analysis of RJEVs

For transmission electron microscope (TEM) analysis, 15 μL of RJEVs was placed on a copper grid and incubated with 15 μL of 2% uranyl acetate aqueous solution for 15 min at room temperature. The number and size distribution of RJEVs were determined using nanoparticle tracking analysis (NTA) with a ZetaView system (Partilce Metrix, Munich, Germany).

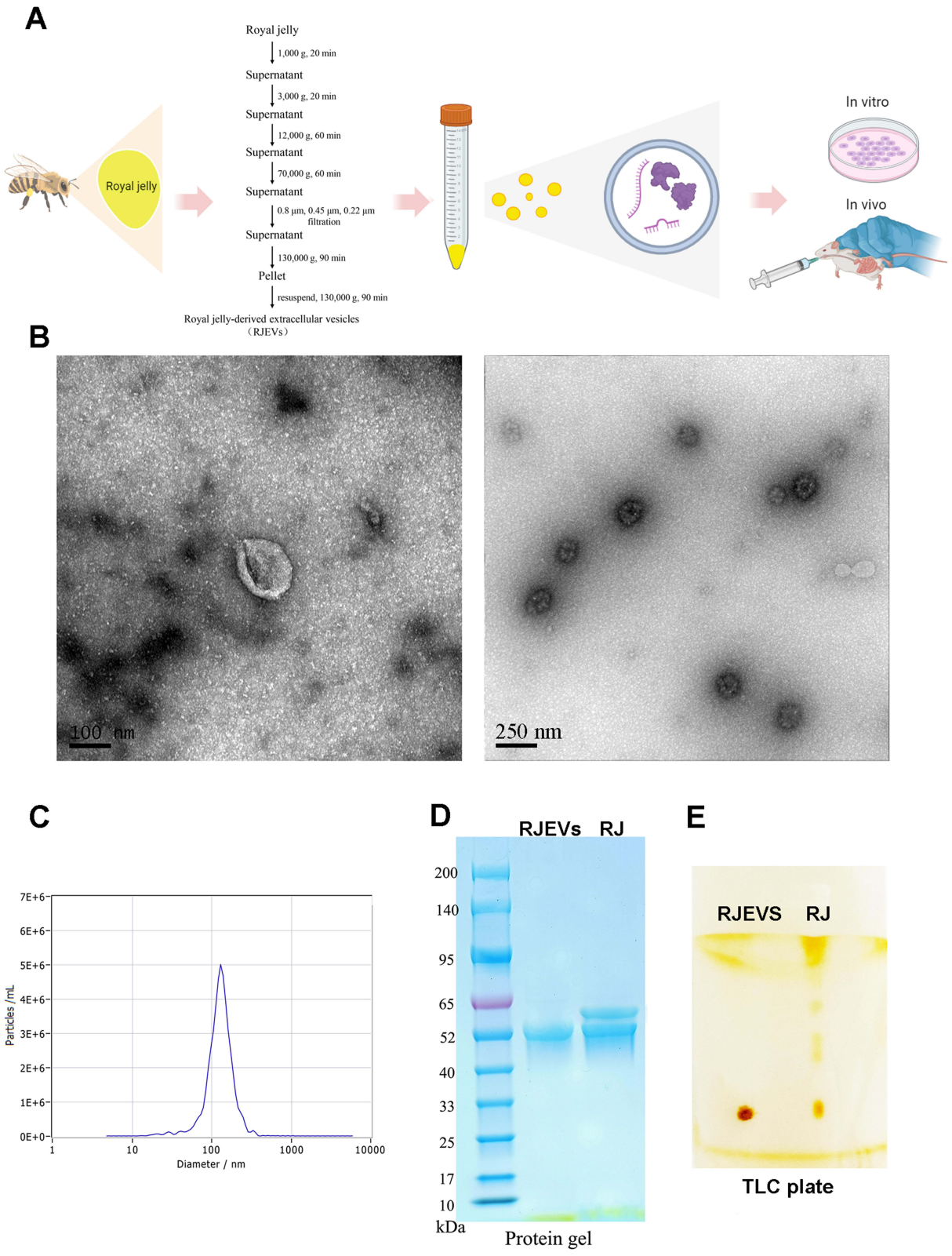

Figure 1 Isolation and characterization of RJEVs. (**A**) Schematic showing the isolation, administration, and antitumor functions of RJEVs in vitro and in vivo. (**B**) Representative ultrastructure TEM image of RJEVs. (**C**) Size distribution and concentration of RJEVs measured using nanoparticle tracking analysis (NTA). (**D**) Protein profile of RJEVs analyzed by SDS-polyacrylamide gel electrophoresis (SDS-PAGE). (**E**) Lipid profile of RJEVs analyzed by TLC.

https://doi.org/10.2147/IJN.S609268

RJEV lipids were extracted with n-hexane for 10 min, after which half of the volume of water was added to the filtrate. The organic phase was collected, dried, and separated on silica gel thin-layer chromatography (TLC) plates using n-hexane/ethyl acetate (8:1) as the developing solvent.

Cells

HepG2 and H22 cell lines (Shanghai Zhong Qiao Xin Zhou Biotechnology Co., Ltd., Shanghai, China) were cultured in tissue culture plates containing Dulbecco's modified Eagle's medium (DMEM) supplemented with 10% heat-inactivated fetal bovine serum (FBS), 100 U/mL penicillin, and 100 μg/mL streptomycin at 37 °C in a 5% CO_2 atmosphere. Cell lines were authenticated by short tandem repeat (STR) profiling and routinely tested for mycoplasma contamination. All experiments were performed using cells within 10 passages after thawing. H22 cells were used exclusively for the in vivo tumor model due to their high tumorigenicity and compatibility with Kunming mice. HepG2 cells were selected for in vitro experiments because their adherent growth.

Mice

Kun-Ming mice (18–22 g) were obtained from Shandong Taibang Biological Products Co., Ltd. (Tai'an, Shandong, China) and housed in a specific pathogen-free (SPF) facility with ad libitum access to deionized water and chow. H22 tumor-bearing mice were generated as previously described.[6] The mice were assigned to five groups (n = 6 per group): (i) normal control (NC), (ii) model control (MC), (iii) positive control (PC), (iv) RJ treatment group (RJ), and (v) RJEV treatment group (RJEV). Mice in the PC group received an intraperitoneal injection of 0.2 mL 5-fluorouracil (20 mg/kg body weight, BW). In the RJ group, mice were gavaged with 0.5 mL RJ solution (3000 mg/kg BW). In the RJEV group, mice were gavaged with a 0.5 mL RJEV suspension (800 mg protein/kg BW). The MC and NC groups received the same volume of PBS via oral gavage. The 800 mg protein/kg dose of RJEVs corresponds to 2000 mg pellet/kg, which is the vesicle fraction isolated from approximately 88.9 g/kg of fresh RJ. A matching crude RJ dose was not feasible due to the physical constraints of oral gavage administration. All treatments were administered once daily for 10 d. At the end of the treatment period, feces were collected under sterile conditions, and the mice were weighed and anesthetized with tribromoethanol. The mice were then sacrificed, and the serum, tumors, liver, and spleen were collected, weighed, and stored for subsequent analysis.

All animal experiments complied with the Animal Research: Reporting of in vivo Experiments (ARRIVE) guidelines and were performed in compliance with the Animal Welfare Committee guidelines and were approved by the Ethics Committee of Shandong Agricultural University (Approval No. SDAU-2019-065).

Preparation of DiR-Labeled RJEVs and Distribution in vivo

To evaluate the in vivo biodistribution, RJEVs were labeled with the near-infrared dye DiR (1,1′-dioctadecyl-3,3,3′,3′-tetramethylindotricarbocyanine iodide; MedChemExpress, Shanghai, China) Briefly, and 2 mg of purified RJEVs suspended in 1 mL PBS was incubated with 1 μL of 1 mM DiR at 37 °C for 20 min, following the manufacturer's protocol. Excess dye was removed by ultracentrifugation at 130,000 × g for 1.5 h. For biodistribution analysis, H22 tumor-bearing mice received a single oral gavage of DiR-labelled RJEVs (800 mg/kg). Whole-body fluorescence imaging was performed 6, 12, and 24 h post-administration using an IVIS Lumina III imaging system (PerkinElmer). At 24 h, the mice were euthanized, and the major organs (liver, spleen, and kidney) and tumors were excised for ex vivo fluorescence quantification. Signal intensities were analyzed using Living Image 4.5 software (PerkinElmer) and normalized to the tissue weight.

Tumor Suppression Rate

Antitumor efficacy was evaluated as tumor inhibition rate, calculated as: Inhibition ratio (%) = (1 – tumor weight (g) of treatment group / tumor weight (g) of model control group (MC)) × 100.

Histological Analysis

For histological evaluation, liver and tumor tissues were fixed in 4% paraformaldehyde, embedded in paraffin, sectioned at 3 μm, stained with hematoxylin and eosin (H&E), and examined under a light microscope (Nikon 80i).

Enzyme-Linked Immunosorbent Assay (ELISA)

Serum cytokine IL-2 and TNF-α levels were quantified using ELISA kits (Shanghai Enzyme-linked Biotechnology Co., Ltd, Shanghai, China) according to the manufacturer's instructions. Briefly, serum samples were centrifuged at 300 × g and the protein concentrations of the supernatants were measured using a BCA Protein Assay Kit (CoWinBioscience, Jiangsu, China). Standards and samples were added to antibody-coated 96-well plates and incubated at 37 °C for 30 min in the dark. After three washes, the avidin–Horseradish Peroxidase (HRP) conjugate and substrate were sequentially added. Absorbance was measured at 570 nm using a microplate reader (SN209595; Agilent BioTek, California, USA).

For oxidative stress analysis, ~0.1 g of liver tissue was homogenized in PBS (1:9, w/v) and centrifuged at 3000 rpm for 10 min at 4 °C. Protein concentrations in the supernatants were measured and total antioxidant capacity (T-AOC), superoxide dismutase (SOD), malondialdehyde (MDA), glutathione peroxidase (GSH-Px), and reduced glutathione (GSH) were determined using commercial kits (Shanghai Enzyme-linked Biotechnology Co., Ltd., Shanghai, China).

Gut Microbiota Analysis

Genomic DNA was extracted from fecal samples using the CTAB method and was used as a template for amplification of the 16S rRNA gene. The V3–V4 regions were amplified by PCR using primers 341F (5′-CCTACGGGNGGCWGCAG -3′) and 806R (5′-GGACTACHVGGGTATCTAAT-3′). Sequencing libraries were prepared using the TruSeq® DNA PCR-Free Sample Preparation Kit (Illumina, USA) and sequenced on an Illumina NovaSeq platform, generating 250 bp paired-end reads at Novogene Technology Co., Ltd. (Beijing, China). Sequences with ≥97% similarity were clustered into operational taxonomic units (OTUs) using Uparse (v7.0.1001). Representative sequences were taxonomically annotated against the Silva database (https://www.arb-silva.de/) using Mothur algorithm. Taxonomic composition and abundance at different ranks (phylum, class, order, family, genus, and species) were determined using the Mothur method and SILVA132 SSU rRNA database. The relative abundance of the bacterial species was visualized using the R software. For differential abundance analysis, the Kruskal–Wallis test was used to compare taxonomic abundances among groups. To control for multiple testing, the Benjamini-Hochberg false discovery rate (FDR) procedure was applied, and adjusted p-values were considered statistically significant.

Short-Chain Fatty Acids Analysis in Feces

Short-chain fatty acids (SCFAs), including acetic, propionic, isobutyric, butyric, isovaleric, and valeric acids, were quantified as the key intestinal metabolites. The SCFA standards (0.1250 g each) were precisely weighed, diluted with ether, and used to establish calibration curves using a gas chromatography–mass spectrometry (GC-MS) system (Trace ISQ 7000, Thermo Fisher, MA, USA). For sample preparation, 0.05 g of mouse feces was dissolved in 10% phosphoric acid, extracted with ether, and centrifuged at 4000 rpm for 15 min. The ether phase was collected for GC-MS analysis and SCFA concentrations were quantified based on standard curves.

Liver Enzymes Analysis

Serum alanine aminotransferase (ALT), aspartate aminotransferase (AST), and lactate dehydrogenase (LDH) levels were measured using an automated biochemical analyzer (7020, Hitachi) with the corresponding standards.

Cell Proliferation

The inhibitory effect of RJEVs on HepG2 cells was evaluated using a Cell Counting Kit-8 (New Cell & Molecular Biotech Co., Ltd., Jiangsu, China). Cells (1×10^4/well in 96-well plates) were cultured in complete medium under 5% CO_2 for 24 h and then serum-starved overnight in a 2% serum medium. Cells were treated with RJEVs (50–1000 μg/mL) for 24 h. Cell viability was assessed according to the manufacturer's protocol and absorbance was measured at 460 nm using a microplate reader. Each concentration was tested in six replicate wells, and the experiment was independently repeated three times.

Acridine Orange and Ethidium Bromide (AO/EB) Fluorescent Dual Staining

Live and dead HepG2 cells were assessed using the AO/EB Kit (Solarbio, Beijing, China). Cells (1×10^6/well in 6-well plates) were cultured and treated as in the proliferation assay, digested with trypsin, and resuspended in PBS at 1×10^6 cells/mL. The cell suspension was stained with AO/EB solution and observed under an inverted fluorescence microscope (TC-S-SR, Nikon).

Flow Cytometry

Apoptosis was evaluated by flow cytometry. HepG2 cells (1×10^6/well in 6-well plates) were cultured and treated as described above. After digestion with trypsin, 1×10^5 cells were resuspended in 100 μL of Annexin V-binding buffer and stained with Annexin V-AbFluor 488 and propidium iodide (PI) for 15 min at room temperature. Data were acquired on a BD LSRFortessa (BD Biosciences, San Jose, CA, USA) and analyzed using FlowJo software. The experiment was independently repeated three times. Early apoptotic cells were defined as Annexin V-positive/PI-negative, and late apoptotic cells as Annexin V-positive/PI-positive.

Gene Activation and Inhibition

For pathway modulation, the PI3K agonist IGF-1 and inhibitor LY194002 were obtained from MedChemExpress (New Jersey, USA). HepG2 cells (1×10^6/well in 6-well plates) were cultured and treated in serum-free medium, as described above. The cells were divided into six groups: (i) normal control (NC), treated with 0.5% dimethyl sulfoxide (DMSO); (ii) agonist group (AG), 0.5% DMSO + IGF-1 (5 ng/mL); (iii) inhibitor group (IN), 0.5% DMSO + LY194002 (50 μM); (iv) RJEVs group, 0.5% DMSO + RJEVs (500 μg/mL); (v) RJEVs + inhibitor group, 0.5% DMSO + RJEVs (500 μg/mL) + LY194002 (50 μM); and (vi) RJEVs + agonist group, 0.5% DMSO + RJEVs (500 μg/mL) + IGF-1 (5 ng/mL). After 48 h, cells were collected for gene and protein expression analyses.

RNA Extraction and Quantitative Real-Time PCR

Total RNA was extracted from RJEVs and murine tumors using a Total RNA Kit (Omega Bio-Tek, Norcross, GA, USA). Briefly, 0.1 g of RJEVs or tumor tissue were disrupted in 1 mL of RNA-Solv Reagent and homogenized. The homogenate was mixed with 200 μL of chloroform and centrifuged, after which ~600 μL of the upper aqueous phase was collected, combined with 200 μL of ethanol, and loaded onto a HiBind® RNA Mini Column. Following centrifugation, the flow-through was discarded and the column was sequentially washed with Wash Buffer I and Wash Buffer II. RNA was eluted with RNase-free water and its quality and concentration were assessed using a NanoDrop spectrophotometer.

For mRNA expression analysis, first-strand cDNA was synthesized from 1 μg of total RNA using the Transcriptor First Strand cDNA Synthesis Kit (Roche, Mannheim, Germany), following the manufacturer's protocol. Quantitative real-time PCR (qPCR) was performed using Top Green qPCR SuperMix (+Dye II; TransGen Biosystems, Foster City, CA, USA). Gene expression was normalized to that of β-actin as an internal reference. All primers were designed and synthesized by Sangon Biotech (Shanghai, China), their sequences are listed in Tables S1 and S2.

Immunofluorescence Analysis

The expression of P85, AKT, caspase-3, and VEGF in tumor tissues was examined by immunofluorescence, following a previously described method.[6] Tumor tissues were fixed in 4% paraformaldehyde, paraffin-embedded, and sectioned. After dehydration and antigen retrieval, nonspecific binding was blocked using bovine serum albumin (BSA). The sections were incubated with primary antibodies overnight at 4 °C, followed by incubation with HRP-conjugated secondary antibodies for 50 minutes at room temperature in the dark. Fluorescence labeling was performed using CY3-TSA, FITC-TSA, and CY5 for sequential antibody detection with microwaving steps between incubations to remove bound primary/secondary antibodies. Nuclei were counterstained with DAPI for 10 min at room temperature. Images were captured using a Panoramic MIDI slice scanner (3DHistech). Antibodies (P85, AKT, caspase-3, and VEGF) and related reagents were purchased from Wuhan ServiceBio Technology Co. Ltd. (Wuhan, China). Primary antibodies were

used at the following dilutions: anti-P85 (1:200), anti-AKT (1:200), anti-caspase-3 (1:500), and anti-VEGF (1:200). Secondary antibodies were used at a dilution of 1:500.

Western Blot Analysis and Commassile Blue Staining

Proteins from cells and tumor tissues were extracted using radioimmunoprecipitation assay lysis buffer (Beyotime Biotechnology, Shanghai, China) supplemented with 1 mM PMSF. Separated proteins were either stained with Coomassie Blue or transferred to nitrocellulose membranes for Western blotting, following a standard protocol. Rabbit polyclonal antibodies against AKT (Cat # AA326), p-AKT (Cat # AA329), p-PI3K (Cat # AF5905), PTEN (Cat # AF1462) and GAPDH (Cat # AF1186) were obtained from Beyotime (Shanghai, China). Protein bands were visualized using NcmECL Ultra detection reagents and imaged using a Fusion Fx System. Primary antibodies were used at the following dilutions: anti-AKT (1:1000), anti-p-AKT (1:1000), anti-p-PI3K (1:1000), anti-PTEN (1:1000), and anti-GAPDH (1:2000). HRP-conjugated secondary antibodies were used at a dilution of 1:5000. Protein bands were quantified by densitometry using ImageJ software (NIH, USA).

Statistical Analysis

All statistical analyses were performed using the SPSS v22.0. Data are expressed as mean ± SEM. Comparisons between three or more groups were performed using one-way ANOVA followed by Tukey's post hoc test. The Student's *t*-test was used for comparisons between two groups. Differences were considered statistically significant at $p < 0.05$. Partial graphics in this document were created using BioRender.com and the necessary publication permission was obtained (Supplementary Material).

Results

RJEVs are Isolated and Characterized

Considering the unique properties of RJ, we optimized EN isolation by modifying established protocols for other bee products (Figure 1A).[21] From 1 g of fresh RJ, approximately 22.5 mg of pelleted RJEVs (wet weight) was obtained. The protein content of the RJEV pellet was approximately 0.4 mg protein per mg of pellet, yielding approximately 9.0 mg of RJEV protein per gram of fresh RJ, as determined by BCA assay.

Comprehensive characterization using multiple complementary techniques. Transmission electron microscopy (TEM) revealed numerous round or cup-shaped nanoparticles with characteristic lipid bilayer membranes (Figure 1B). The background was relatively clean, with minimal visible amorphous material, further supporting the purity of the preparation. Nanoparticle tracking analysis (NTA) confirmed size distribution and concentration, yielding 4.8×10^{10} particles/mL from 6 g of RJ. RJEVs displayed a peak particle size of 136.2 nm and a mean size of 126 nm, with 97.5% of particles ranging from 76.5–132 nm (Figure 1C).

To further probe RJEV composition, we evaluated the protective capacity of the membranes against RNA degradation. Protein analysis using Sodium dodecyl sulfate–polyacrylamide gel electrophoresis (SDS-PAGE) and Coomassie staining revealed bands predominantly in the 50–60 kDa range (Figure 1D), and individual proteins were identified and quantified (Table S3 and Figure S1). Thin-layer chromatography (TLC) analysis showed that RJEV lipids were less diverse than those in the crude RJ (Figure 1E). Collectively, the presence of a characteristic lipid bilayer membrane observed by TEM, the homogeneous nano-scale size distribution confirmed by NTA, and the distinct protein and lipid profiles relative to crude RJ demonstrate that the isolated RJEVs are vesicular in nature and are not dominated by co-isolated soluble proteins or non-specific aggregates.

RJEVs Exhibit Organ-Specific Biodistribution Patterns in H22 Tumor-Bearing Mice

Following oral treatment, DiR-labeled RJEVs were localized exclusively in the abdominal region of mice (Figure 2A). Fluorescence peaked 12 h post-gavage and declined thereafter (Figure 2B). At 24 h, the results revealed preferential accumulation of fluorescence signal in the liver and, to a lesser extent, in tumor tissues, whereas signals in the spleen and kidney were negligible (Figure 2C). These observations indicate that RJEVs are capable of reaching the liver and tumor

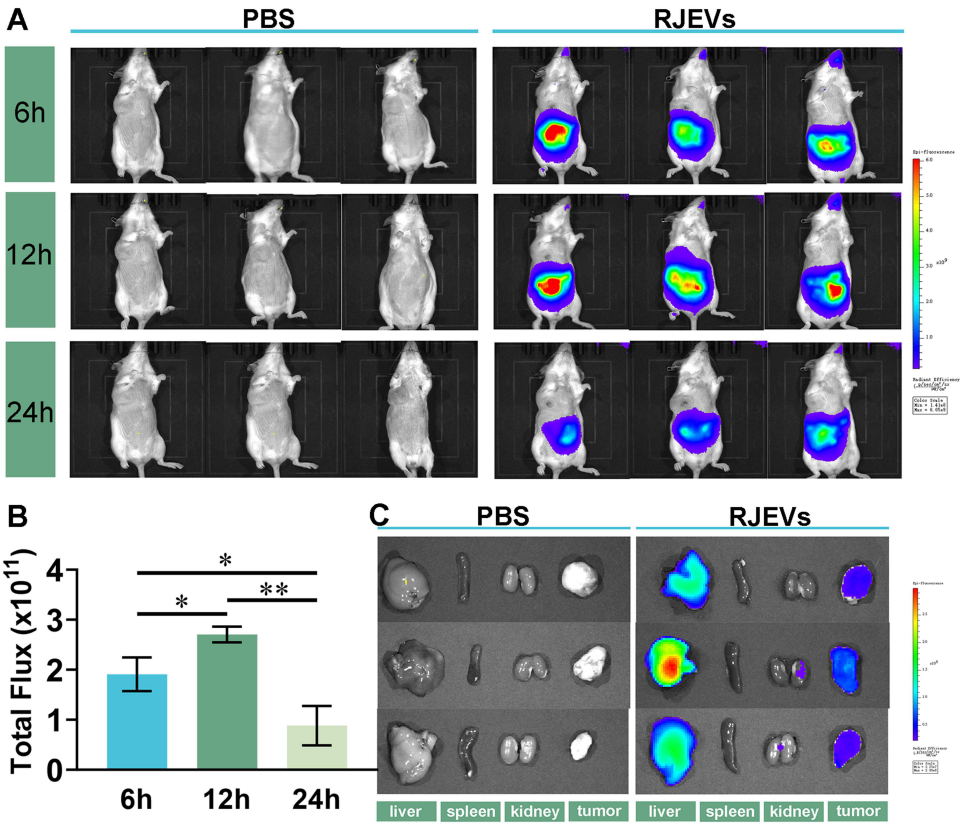

Figure 2 Biodistribution of orally administered RJEVs in vivo. (**A**) Biodistribution of RJEVs in mice at 6h, 12h, and 24 h post-oral administration. (**B**) Total fluorescence intensity quantified using the in vivo imaging system. (**C**) Ex vivo images of major organs (tumor, spleen, kidney) and tumor tissues at 24 h post-administration. Data were presented as mean ± SEM (n = 3); *p < 0.05, **p < 0.01.

sites following oral administration. However, given the absence of a free DiR dye control, we cannot completely exclude the possibility that a minor portion of the liver signal may originate from residual free dye; nonetheless, the prolonged tissue retention and the detection of signal in subcutaneous tumor tissues support that the observed biodistribution primarily reflects intact RJEVs. This dual tropism may underlie their hepatoprotective effects in tumor-bearing mice while simultaneously inducing apoptosis in tumor cells.

RJEVs Exhibit Significant Antitumor Effects and Promote Tumor Cell Death Apoptosis in vivo

To evaluate the antitumor efficacy of RJEVs, we analyzed body weight before and after treatment, as well as liver and spleen indices at the study endpoint (Figure S2). The tumor weight was measured in tumor-bearing mice, and the suppression rate was calculated. RJEVs treatment significantly reduced tumor weight compared to the MC group ($p < 0.05$), achieving a tumor inhibition rate of 41.15% (Table 1). This inhibition rate, while moderate compared to the chemotherapeutic agent 5-FU (67.90%), was achieved through oral administration of unmodified natural nanovesicles. Notably, RJEVs demonstrated stronger tumor-suppressive activity than RJ did. Histopathological assessment further confirmed that HE-stained tumor sections from the MC group showed densely arranged neoplastic cells with distinct borders and prominent nucleoli, whereas the PC, RJ, and RJEVs groups exhibited varying degrees of necrosis, characterized by disrupted membranes, pyknotic nuclei, and cytoplasmic vacuolation (Figure 3A). These histological findings corroborated the suppression data, collectively highlighting the potent antitumor effects of the RJEVs.

Table 1 Effects of Different Treatments on Tumor Weight and Inhibition Rate of Tumor Growth in H22 Tumor-Bearing Mice

Group	Tumor Weight (g)	Inhibition Ratio (%)
MC	1.37±0.20	–
PC	0.44±0.06**	67.90
RJ	0.92±0.19	32.47
RJENs	0.80±0.13*	41.15

Notes: Results are expressed as mean ± SEM (n = 6). Data were analyzed by one-way ANOVA and Tukey post-hoc test; *p < 0.05, **p < 0.01, compared with the MC group.

RJEVs Ameliorated Hepatic Injury and Enhanced Both Antioxidant Capacity and Immune Function in H22 Tumor-Bearing Mice

Serum ALT, AST, and LDH levels, key indicators of hepatic injury, were quantified to assess tumor-induced hepatotoxicity.[23] Tumor-bearing mice displayed elevated serum levels of all three markers compared to the NC group (Figure 3B), confirming substantial liver damage. Importantly, RJEVs treatment significantly reduced ALT, AST, and LDH levels compared with those in the MC group, demonstrating marked hepatoprotective activity. RJEVs also outperformed RJ in normalizing ALT and AST

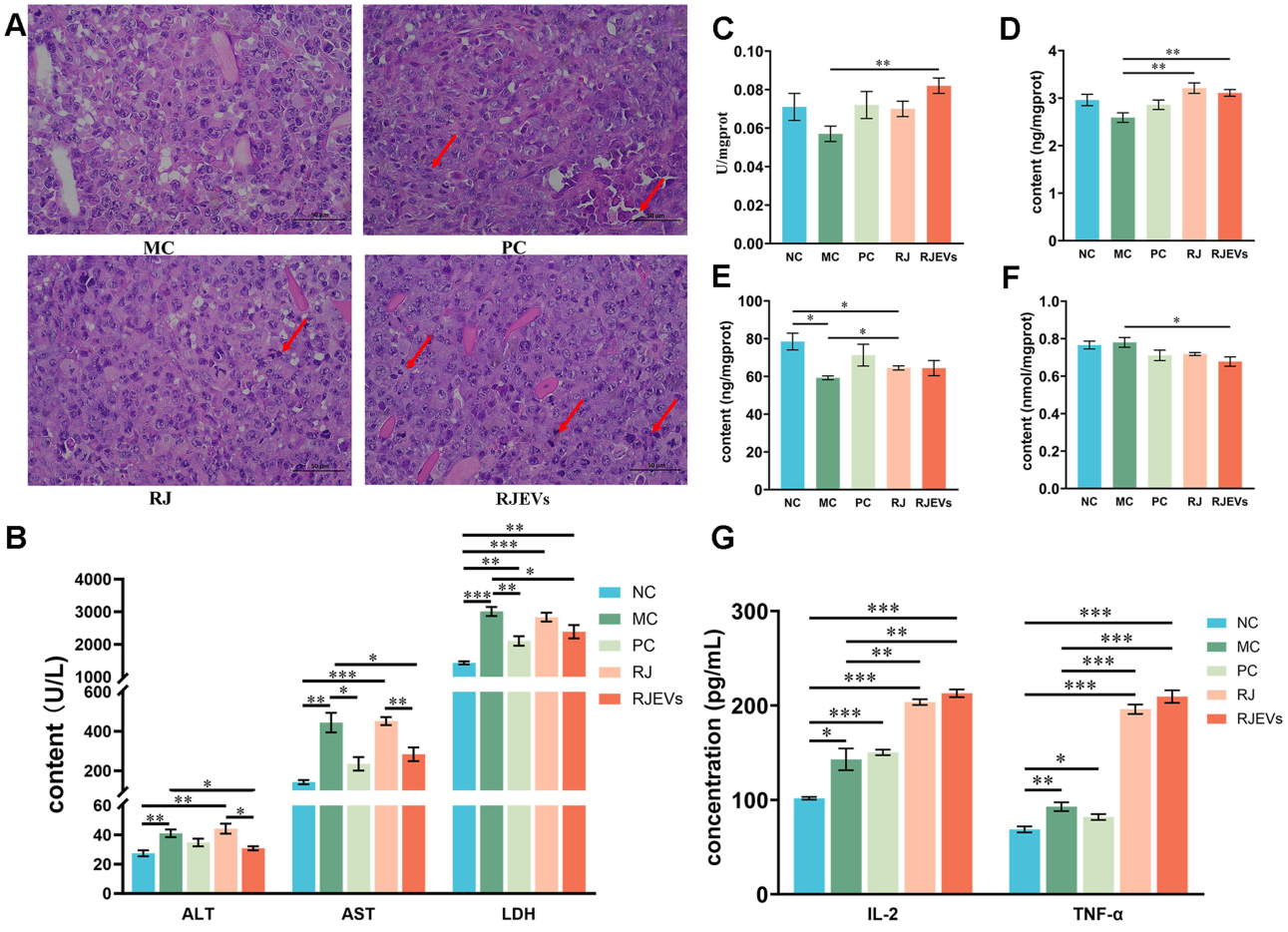

Figure 3 In vivo antitumor efficacy of RJEVs in H22 tumor-bearing mice. (**A**) Histological examination of the morphological changes in tumors harvested from H22-bearing mice for H&E staining (400×). The changes in the tumor cells are marked by arrow heads. (**B**) Content of serum biochemical markers of hepatic injury (ALT, AST and LDH) in serum. (**C**–**F**) T-AOC activity, and the content of SOD, GSH-Px, and MDA in liver tissue. (**G**) Content of IL-2 and TNF-α in serum. Data were presented as mean ± SEM (n = 6); *p < 0.05, **p < 0.01, ***p < 0.001.

https://doi.org/10.2147/IJN.S609268

levels, suggesting that RJEVs may represent a critical therapeutic fraction that mediates RJ's antitumor efficacy of RJ (Figure 3B). Collectively, these results demonstrated that RJEVs attenuated hepatic injury associated with subcutaneous H22 hepatocellular carcinoma progression in mice.

Because antioxidant enzymes preserve hepatocyte integrity by eliminating reactive oxygen species (ROS) and preventing lipid peroxidation, we further evaluated hepatic antioxidant capacity by quantifying T-AOC, SOD, GSH-Px, and MDA levels. While 5-FU (PC) showed the strongest tumor-suppressive activity, RJEVs exhibited superior antioxidant enhancement compared with the MC group. Specifically, RJEVs increased T-AOC and SOD activities and decreased MDA content, thereby reinforcing hepatic antioxidant defenses in H22 tumor-bearing mice (Figure 3C–F).

We next examined the immunomodulatory role of RJEVs by measuring serum IL-2 and TNF-α, two cytokines central to antitumor immunity.[24] Tumor development markedly increased both cytokines, and although 5-FU failed to alter their levels relative to the MC group, RJ and RJEVs significantly elevated them (Figure 3G). These findings indicate that RJEVs exert antitumor effects partly through immunomodulation, a mechanism distinct from the direct cytotoxicity of 5-FU.

RJEVs Regulate the Gut Microbiota and SCFA Metabolism in Tumor-Bearing Mice

To investigate the impact of RJEVs on the gut microbiota, we performed family level taxonomic profiling. The top 10 most abundant bacterial families revealed that both tumorigenesis and treatment markedly altered microbial composition (Table S4 and Figure 4A). Quantitative analysis of the dominant families (>5% relative abundance) identified five key groups: *Muribaculaceae, Lactobacillaceae, Bacteroidaceae, Lachnospiraceae*, and *Rikenellaceae* (Figure 4B–F). Compared to NC mice, the MC group showed an increased *Lachnospiraceae* and *Rikenellaceae* but a reduced *Lactobacillaceae* and *Bacteroidaceae*. RJEVs intervention was associated with a partial restoration of the microbiota profile toward that of NC mice (Figure 4C–F). Comparative analysis of RJ and RJEVs identified nine families with differential abundances. *Muribaculaceae, Lactobacillaceae*, and *Bacteroidaceae* were the most abundant. RJEVs treatment was associated with significantly higher relative abundances of *Muribaculaceae* and *Bacteroidaceae* compared with RJ treatment (Figure 4G).

Given the role of gut microbiota–derived SCFAs in modulating host immunity, we quantified fecal SCFAs.[25] Tumor development markedly disrupted SCFA profiles (Figure 4H–M). RJEVs did not reverse most tumor-induced alterations (acetic, propionic, isobutyric, butyric, isovaleric, and valeric acids) except for butyric acid. Instead, RJEVs further increased propionic acid, isobutyric acid, and valeric acid concentrations. Comparative analysis revealed that, despite RJEVs being derived from RJ, their effects on SCFA profiles diverged substantially, underscoring the mechanistic differences in their biological activities.

To further clarify the relationship between gut microbiota and short-chain fatty acids (SCFAs) in mice, we performed Pearson correlation analyses between SCFAs and gut microbial families with a relative abundance of >1%. The results showed that fecal concentrations of acetic acid and butyric acid were positively correlated with *Bacteroidaceae, Helicobacteraceae*, and *Prevotellaceae*. In contrast, propionic, isobutyric, isovaleric, and valeric acids were positively associated with Muribaculaceae abundance. Notably, propionic acid and isobutyric acid were negatively correlated with *Lactobacillaceae* and *Staphylococcaceae* (Figure 4N). Collectively, these correlative findings suggest that RJEVs may modulate the gut microbiota and SCFA metabolism as part of a systematic, multifaceted antitumor process; however, causal relationships between specific microbial changes and antitumor outcomes remain to be established through interventional approaches.

RJEVs Exert Antitumor Effects Through the PI3K/AKT and VEGF Pathways

To further determine whether the tumor cell death observed by histology involved apoptosis, building on our previous observation that RJ exerts antitumor effects through the PI3K/AKT and VEGF pathways, we systematically examined the regulatory role of RJEVs on these oncogenic cascades.[6] Compared with the MC group, both the PC and RJEVs groups markedly altered the expression of PI3K/AKT- and VEGF-related genes and proteins (Figure 5). Specifically, P85, AKT, COX-2, and VEGF expressions decreased, whereas Bax expression increased in the PC and RJEVs groups (Figure 5A–H). In contrast, RJ alone had no significant effect on P85, AKT, caspase-9, caspase-3, PTEN, Bax, COX-2, or VEGF expression (Figure 5A–H). Comparative analysis revealed that RJEVs significantly upregulated caspase-3 expression (Figure 5D).

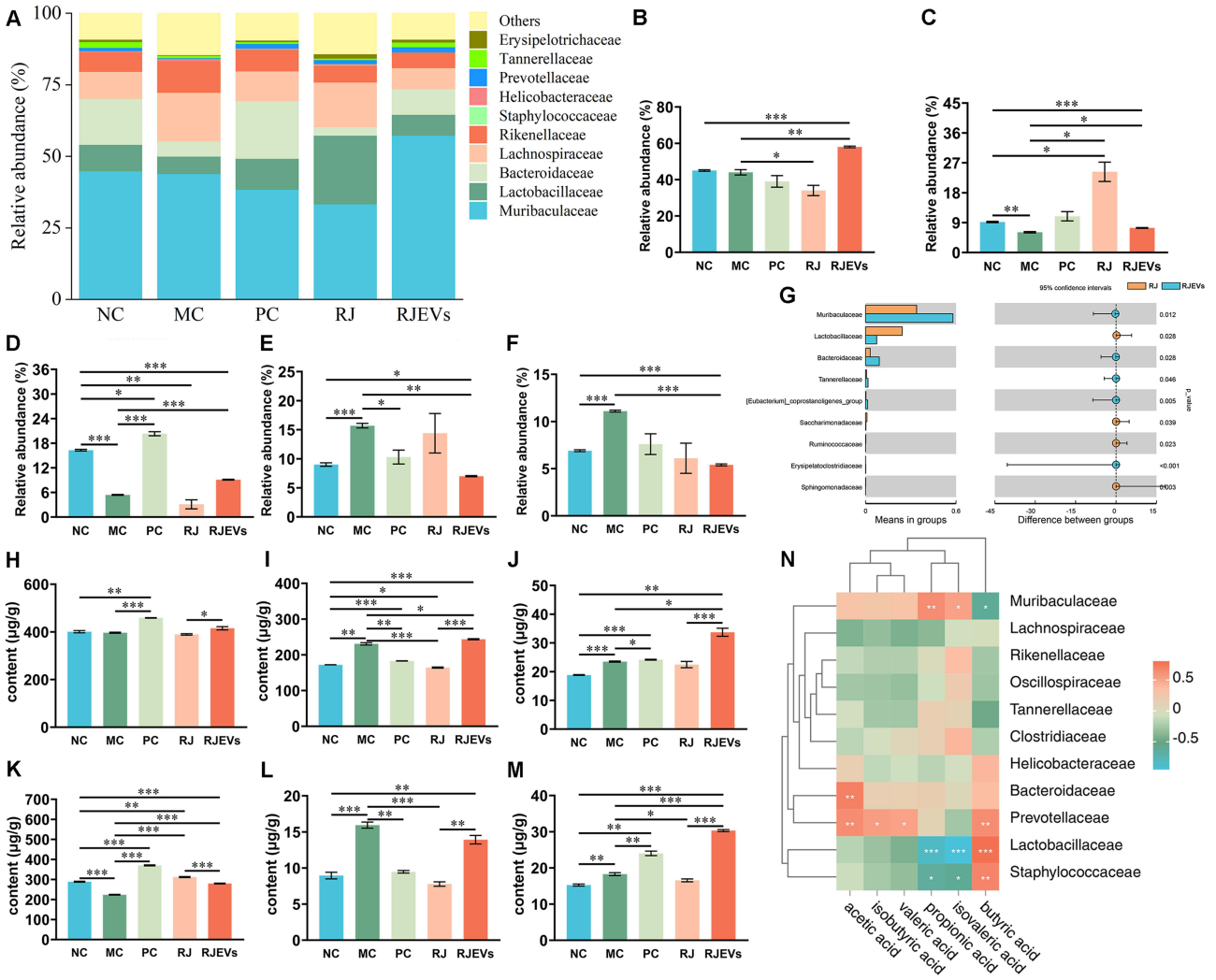

Figure 4 Gut microbiota profiling and short-chain fatty acid (SCFA) analysis in H22 tumor-bearing mice. (**A**) Taxonomic composition of fecal microbiota at the family level. (**B**–**F**) Relative abundance of Muribaculaceae, Lachnospiraceae, Bacteroidaceae, Lactobacillaceae, and Rikenellaceae in different treatments. (**G**) Differential abundance analysis of bacterial taxa between RJ and RJEVs treatment groups at the family level. (**H**–**M**) Content of acetic acid, propionic acid, isobutyric acid, butyric acid, isovaleric, and valeric acid with different treatments. (**N**) Correlation analysis between the abundance of gut microbiota at the family level and content of SCFA in feces. Data were presented as mean ± SEM (n = 6); *p < 0.05, **p < 0.01, ***p < 0.001.

To more intuitively observe the expression of proteins associated with the PI3K/AKT and VEGF signaling pathways, immunofluorescence was used to analyze the expression levels of P85, AKT, and caspase-3 in tumor tissues. Optical density quantification confirmed that RJEVs and PC treatment significantly downregulated P85 and AKT while upregulating caspase-3 (Figure 5I–O). These results demonstrated consistent regulatory trends in gene and protein expression.

RJEVs Induced Apoptosis in HepG2 Cells Through PI3K/AKT Signaling Pathway in vitro

Given the in vivo evidence of RJEV-mediated apoptosis in hepatocellular carcinoma (HCC), we performed mechanistic in vitro studies using HepG2 cells. A series of assays, including CCK-8, AO/EB dual staining, flow cytometry, and live/dead staining, were conducted to determine the optimal apoptotic concentration of RJEVs. Across independent experiments, RJEV-induced apoptosis in HepG2 cells showed no clear dose dependency (0–1000 μg/mL). However, 500 μg/mL produced the strongest anti-proliferative and pro-apoptotic effects (Figure 6A, M and N; Figure S3) and was therefore selected for subsequent experiments.

https://doi.org/10.2147/IJN.S609268

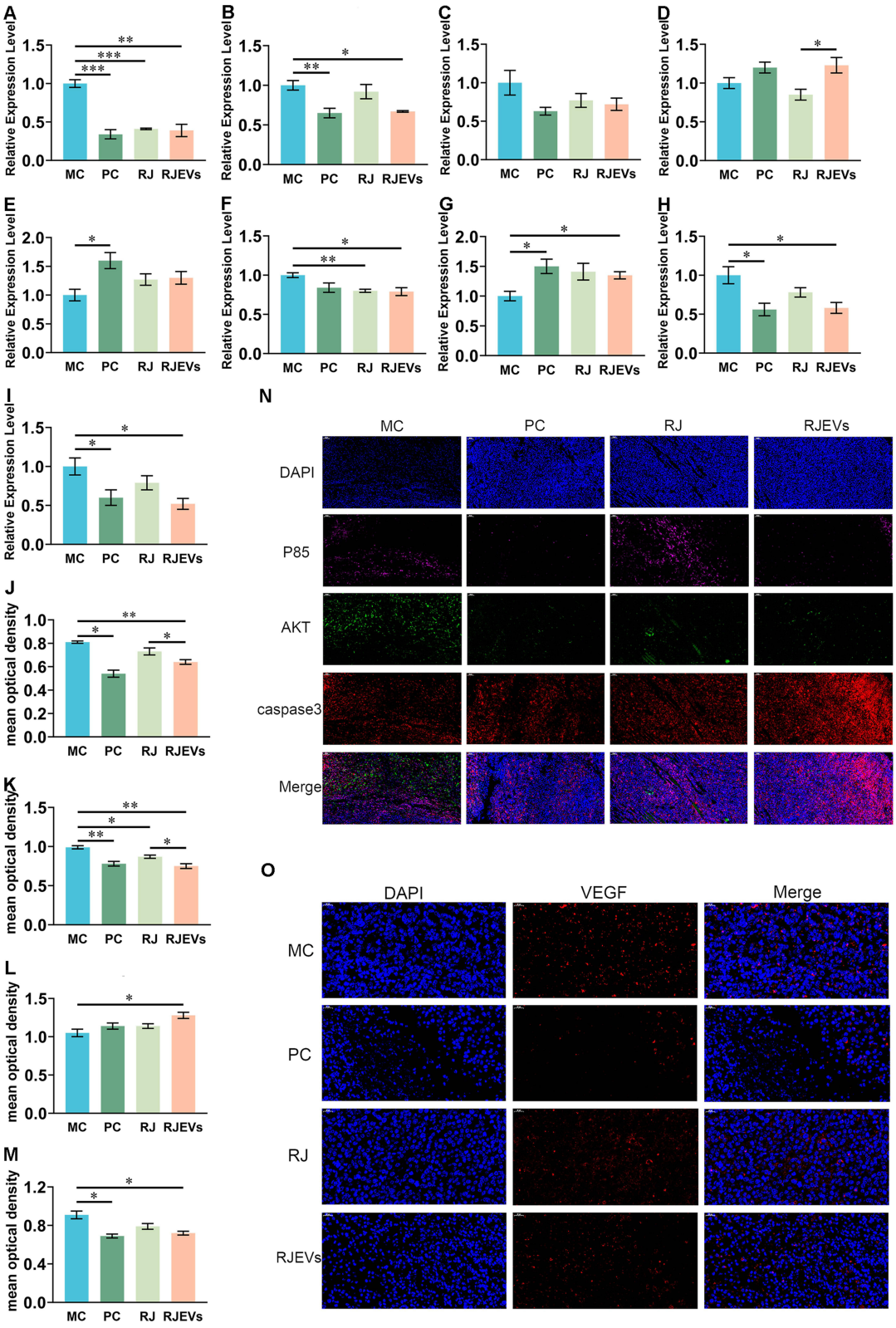

Figure 5 Expression level of gene and protein in the PI3K/AKT signaling pathway in H22 tumor-bearing mice. (**A–I**) Relative expression levels of P85, AKT, caspase9, caspase3, PTEN, Bcl-2, Bax, COX-2 and VEGF genes in different treatments. (**J–M**) Mean optical density of P85, AKT, caspase3 and VEGF protein. (**N** and **O**) The expression of P85, AKT, caspase3 and VEGF was examined by immunofluorescence. Data were presented as mean ± SEM (n = 6); *p < 0.05, **p < 0.01, ***p < 0.001.

https://doi.org/10.2147/IJN.S609268

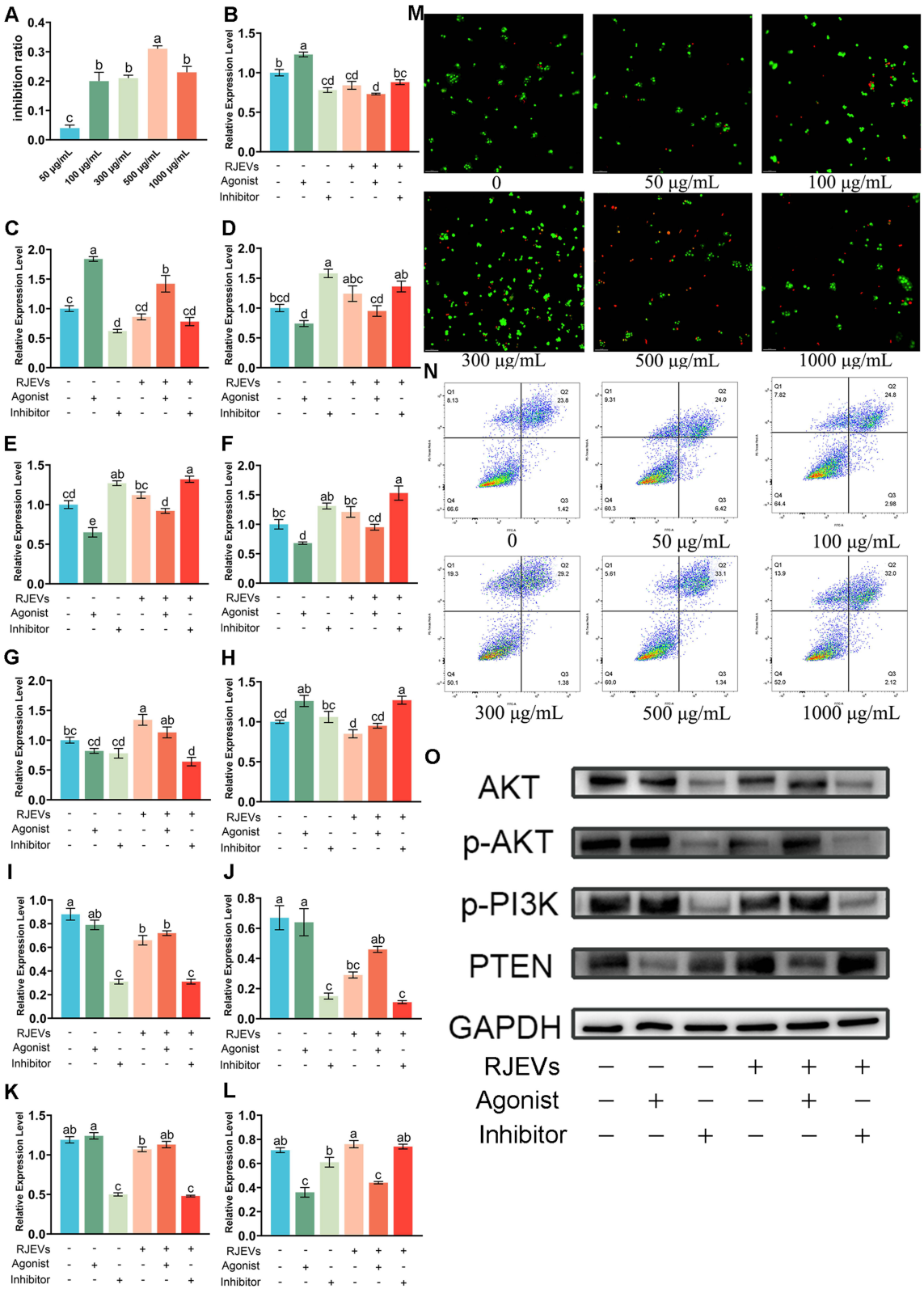

Figure 6 Optimization of RJEVs concentration in HepG2 cells and regulatory mechanisms on the PI3K/AKT signaling pathway. (**A**) CCK-8 assay for screening optimal dosage of RJEVs in vitro. (**B**–**H**) The expression level of P85, AKT, caspase 9, caspase 3, PTEN, Bax and Bcl-2 genes in HepG2 cells following the administration of inhibitors and agonists. (**I**–**L**) Expression level of AKT, p-AKT, p-PI3K and PTEN protein in HepG2 cells following the administration of inhibitors and agonists. (**M**) AO/EB fluorescent dual staining for screening optimal dosage of RJEVs in vitro. (**N**) Flow cytometry for screening optimal dosage of RJEVs in vitro. (**O**) Immunoblotting of the expression of AKT, p-AKT, p-PI3K, and PTEN proteins. Data were presented as mean ± SEM (n = 6); Different lowercase letters (a–e) above the bars indicate statistically significant differences between groups ($p < 0.05$). Symbols "+" and "–" denote the presence or absence of RJEVs, IGF-1, or LY294002 as indicated.

https://doi.org/10.2147/IJN.S609268

To verify whether the PI3K/AKT pathway mediates RJEV-induced apoptosis, HepG2 cells were treated with PI3K agonists and inhibitors. Gene expression analysis showed that pathway activation or inhibition modulated downstream targets. RJEVs significantly suppressed P85 expression and enhanced Bax expression. Co-treatment with agonists or inhibitors reversed the agonist-driven effects on P85, AKT, Bax, Bcl-2, and caspase-3 while synergistically amplifying the inhibitory effect on Bcl-2. At the protein level, RJEVs reduced AKT and p-AKT levels, while upregulating PTEN expression. Importantly, RJEVs combined with inhibitors produced more pronounced regulatory effects than RJEVs alone (Figure 6B–L and O).

Discussion

Our findings provide evidence that RJEVs represent a functionally important fraction contributing to the antitumor and other pharmacological activities of RJ. Although RJEVs have a simpler composition than whole RJ, their anti-HCC effects in mice involve complex synergistic processes that integrate immune modulation, metabolic reprogramming, and gut microbiota regulation. These systemic effects ultimately converge on PI3K/AKT signaling, driving apoptosis in HCC cells. This study opens new avenues for exploring the molecular mechanisms by which insect- or plant-derived ENs communicate with mammalian systems. Although we did not investigate the specific regulatory components of RJEVs (eg, miRNAs) at a mechanistic level, we established their systemic antitumor efficacy and multilayered regulatory roles in vivo. Importantly, the demonstrated modulation of PI3K/AKT signaling provides a strong theoretical foundation for future research on miRNA-targeted delivery and the use of RJEVs as natural nanocarriers.

The present findings build directly upon our previous work, in which we demonstrated that crude RJ and selenium-enriched RJ suppress HCC progression through the PI3K/AKT and VEGF pathways in the same H22 tumor-bearing mouse model.[6] However, that study treated RJ as a complex whole substance and did not identify which specific constituents were responsible for the observed antitumor activity. The current study advances this finding by isolating and functionally characterizing RJEVs as a specific nanoscale fraction that contributes significantly to the anti-HCC effects of RJ. This represents a logical progression from studying crude mixtures toward identifying purified bioactive constituents, analogous to the historical development of natural product pharmacology.

Exosomes or exosomes-like nanoparticles are produced by most organisms, including animals, plants and microbes.[26] Current preparation methods for food- or plant-derived ENs include ultracentrifugation, ultrafiltration, size-exclusion chromatography, and immunoaffinity enrichment, among others.[27] The choice of isolation method often depends on the source material, though differential ultracentrifugation combined with density gradient centrifugation remains the most widely used strategy. Fresh RJ is a viscous nutrient-rich substance that contains proteins, carbohydrates, lipids, and other bioactive molecules. In our experiments, we evaluated multiple methods to isolate RJEVs. Ultrafiltration and immunoaffinity enrichment proved to be inadequate for the removal of abundant protein impurities. By adapting ultracentrifugation protocols originally developed for the isolation of milk exosomes, we obtained high-purity RJEVs using a 70,000 × g ultracentrifugation step coupled with gradient filtration membranes.[28]

Although previous studies have reported exosome-like vesicles in RJ and analyzed their antibacterial and pro-regenerative activities, our morphological characterization of RJEVs showed partial discrepancies with earlier findings.[21] Using both TEM and NTA, we confirmed that RJEVs have an average diameter of ~130 nm, consistent with exosomal size profiles.[9] High-resolution TEM imaging further revealed the detailed morphological features of RJEVs. Biochemical analysis confirmed that RJEVs contain proteins and lipids, with the latter forming a bilayer structure essential for vesicle stability, uptake, and other biological functions.[29,30] Unlike typical exosomes, which contain diverse transmembrane and membrane-associated proteins, RJEVs exhibit a simpler protein composition and a more homogeneous lipid profile relative to whole RJ. This streamlined molecular makeup facilitates mechanistic studies and supports the notion that the physiological functions of RJ may depend on specific nanovesicle components, rather than on the crude mixture.

Organisms maintain homeostasis and suppress oncogenic transformations through coordinated immune responses, antioxidant defense, and other systemic regulatory processes. The tumor inhibition rate of RJEVs (41.15%) exceeded that of crude RJ (32.47%), despite the fact that the RJEV dose corresponded to the vesicle fraction isolated from approximately 88.9 g/kg of fresh RJ—nearly 30-fold higher than the crude RJ dose of 3 g/kg actually administered. This substantial dose difference, arising from the physical impossibility of administering crude RJ at a matched dose due to its viscosity and volume, underscores the potency

and enrichment of bioactivity in the vesicle fraction. It should also be noted that the tumor inhibition rate of approximately 41.15% achieved by RJEVs is moderate compared to that of the conventional chemotherapeutic agent 5-FU (67.9%). However, these two treatments appear to act through fundamentally different mechanisms. The anti-metabolite 5-Fu, long established as a chemotherapeutic agent, exerts cytotoxicity by generating active metabolites that inhibit thymidylate synthase and incorporate it into DNA and RNA, thereby disrupting mitosis and blocking cell proliferation.[31,32] This explains why 5-Fu did not enhance the immune function in tumor-bearing mice. In contrast, RJEVs simultaneously enhanced host immune function, improved hepatic antioxidant capacity, and modulated the gut microbiota—effects that are not captured by the tumor inhibition rate alone. This multimodal activity profile suggests that RJEVs may be particularly suitable for development as part of combinatorial strategies, such as an adjuvant to conventional chemotherapy or as a component of integrative oncology approaches. Biodistribution studies have revealed a substantial hepatic accumulation of RJEVs, accounting for their pronounced effects on liver-related biomarkers. Moreover, RJEVs exhibited superior antitumor efficacy compared to whole RJ. Although RJ's antitumor activity of RJ has been well documented, its mechanisms have rarely been explored at the nanovesicle level.[5,33] Our findings suggest that RJEVs serve as functional carriers that mediate RJ's pharmacological effects of RJ.

The gut microbiota analysis in this study was not designed as an isolated experiment, but was intended to illustrate that the antitumor effects of RJEVs involve a systematic, multifaceted process extending beyond direct tumor cell killing. The liver is tightly linked to the gut microbiota through the gut–liver axis, which governs homeostasis and contributes to liver disease pathogenesis.[34] Patients with hepatocellular carcinoma (HCC) display distinct microbial signatures compared with non-HCC controls, supporting the role of microbiota-driven pathways in HCC development.[35,36] Among commensals, Muribaculaceae have gained attention for their beneficial roles in host health.[37] Our data showed that RJEVs significantly increased Muribaculaceae abundance in tumor-bearing mice. This family specializes in degrading complex polysaccharides into short-chain fatty acids (SCFAs), such as acetate and propionate.[38,39] RJEVs treatment markedly increased fecal levels of propionate, butyrate, and valerate, and correlation analyses confirmed strong positive associations between Muribaculaceae abundance and SCFA concentrations. Conversely, in our dataset, the families *Lachnospiraceae* and *Rikenellaceae* positively correlated with tumorigenesis. Comparative analyses revealed that RJEVs outperform RJ in promoting *Muribaculaceae* enrichment and SCFA production. Collectively, these correlative results suggest that RJEVs may influence the gut–liver axis, and this potential modulation warrants further investigation. Interventional studies, such as fecal microbiota transplantation or antibiotic depletion experiments, will be necessary to determine whether RJEV-induced changes in gut microbiota and SCFA metabolism directly contribute to the antitumor effects or represent secondary phenomena.The PI3K/AKT signaling pathway is a key oncogenic transduction cascade that amplifies the Warburg effect, thereby promoting tumor growth and metastasis.[40] Dysregulation of PI3K is among the most frequent events in tumorigenesis, with particularly high expression observed in HCC tissues.[41,42] In the present study, we detected marked hyperactivation of the PI3K regulatory subunit P85 in the PC group, consistent with tumor-driven signaling alterations. Our previous work demonstrated that RJ induces tumor cell apoptosis via the PI3K/AKT axis and suppresses tumor angiogenesis through the VEGF pathway.[6] Building on this, we now show that RJEVs exert antitumor activity by concurrently inhibiting the PI3K/AKT and VEGF signaling pathways. Mechanistic validation was achieved by culturing HepG2 cells in vitro and modulating the PI3K/AKT activity through pharmacological activation and inhibition. Since aberrant activation of PI3K/AKT occurs in nearly 50% of HCCs, our findings highlight the therapeutic promise of RJEVs for designing targeted PI3K/AKT inhibitors and developing safe and effective treatment strategies for patients with advanced HCC ineligible for resection.[43]

Conclusion

In conclusion, RJEVs exhibited significant antitumor efficacy in both in vivo and in vitro models, with effects that were comparable to or exceeded those of crude RJ across multiple parameters. These findings position RJEVs as important bioactive constituents that contribute to the anticancer effects of RJ and highlight the value of studying specific nanoscale fractions of natural products to identify potent bioactive components. Unlike the single-target mechanism of 5-FU, RJEVs act through a multifaceted regulatory process: enhancing systemic antioxidant and immune responses, reshaping gut microbiota and its metabolites, and ultimately inducing tumor apoptosis via PI3K/AKT signaling. The moderate tumor inhibition rate, coupled with the multifaceted systemic benefits observed, suggests that RJEVs may have particular

value as part of integrative or combinatorial therapeutic strategies. Importantly, EVs or ENs can facilitate interspecies communication by transferring diverse cargoes, including proteins, lipids, and nucleic acids, from plant or insect cells to mammalian cells. However, the precise components of RJEV that drive their antitumor effects remain to be elucidated. Given the natural origin and biocompatibility of RJ, RJEVs hold promise as biofunctional delivery nanoplatforms for future development. While the present study focuses on the endogenous bioactivity of RJEVs, their demonstrated ability to reach the liver and tumor tissues following oral administration provides a foundation for future engineering of RJEV-based therapeutics with targeted and multifunctional applications in cancer therapy.

Acknowledgments

This work was funded by the National Natural Science Foundation of China (32302811), Shandong Provincial Natural Science Foundation (ZR2022QC071), and Earmarked Fund for Agriculture Research System of China (CARS-44).

Disclosure

The authors report no conflicts of interest in this work.

References

1. Atanasov AG, Zotchev SB, Dirsch VM, et al. Natural products in drug discovery: advances and opportunities. *Nat Rev Drug Discov*. 2021;20(3):200–216. doi:10.1038/s41573-020-00114-z
2. Kunugi H, Mohammed Ali A. Royal jelly and its components promote healthy aging and longevity: from animal models to humans. *Int J Mol Sci*. 2019;20(19):4662. doi:10.3390/ijms20194662
3. Chi X, Liu Z, Wang H, et al. Royal jelly enhanced the antioxidant activities and modulated the gut microbiota in healthy mice. *J Food Biochem*. 2021;45(5):e13701. doi:10.1111/jfbc.13701
4. Fratini F, Cilia G, Mancini S, et al. Royal Jelly: an ancient remedy with remarkable antibacterial properties. *Microbiol Res*. 2016;192:130–141. doi:10.1016/j.micres.2016.06.007
5. Oršolić N, Jazvinšćak Jembrek M. Royal jelly: biological action and health benefits. *Int J Mol Sci*. 2024;25(11):6023.
6. Chi X, Liu Z, Wei W, et al. Selenium-rich royal jelly inhibits hepatocellular carcinoma through PI3K/AKT and VEGF pathways in H22 tumor-bearing mice. *Food Funct*. 2021;12(19):9111–9127. doi:10.1039/D1FO01070K
7. Keller S, Sanderson MP, Stoeck A, et al. Exosomes: from biogenesis and secretion to biological function. *Immunol Lett*. 2006;107(2):102–108. doi:10.1016/j.imlet.2006.09.005
8. Valadi H, Ekström K, Bossios A, et al. Exosome-mediated transfer of mRNAs and microRNAs is a novel mechanism of genetic exchange between cells. *Nat Cell Biol*. 2007;9(6):654–659. doi:10.1038/ncb1596
9. Kalluri R, LeBleu VS. The biology, function, and biomedical applications of exosomes. *Science*. 2020;367(6478). doi:10.1126/science.aau6977
10. Munir J, Lee M, Ryu S. Exosomes in food: health benefits and clinical relevance in diseases. *Adv Nutr*. 2020;11(3):687–696. doi:10.1093/advances/nmz123
11. Teng Y, Ren Y, Sayed M, et al. Plant-derived exosomal MicroRNAs shape the gut microbiota. *Cell Host Microbe*. 2018;24(5):637–652.e638. doi:10.1016/j.chom.2018.10.001
12. Mu J, Zhuang X, Wang Q, et al. Interspecies communication between plant and mouse gut host cells through edible plant derived exosome-like nanoparticles. *Mol Nutr Food Res*. 2014;58(7):1561–1573. doi:10.1002/mnfr.201300729
13. Hwang JH, Park YS, Kim HS, et al. Yam-derived exosome-like nanovesicles stimulate osteoblast formation and prevent osteoporosis in mice. *J Control Release*. 2023;355:184–198. doi:10.1016/j.jconrel.2023.01.071
14. Liao YT, Liu CH, Yu J, et al. Liver cancer cells: targeting and prolonged-release drug carriers consisting of mesoporous silica nanoparticles and alginate microspheres. *Int J Nanomed*. 2014;9:2767–2778. doi:10.2147/IJN.S60171
15. Li Z, Bao H. Anti-tumor effect of Inonotus hispidus petroleum ether extract in H22 tumor-bearing mice and analysis its mechanism by untargeted metabonomic. *J Ethnopharmacol*. 2022;285:114898. doi:10.1016/j.jep.2021.114898
16. Qu Y, Li C, Zhang C, et al. Optimization of infrared-assisted extraction of Bletilla striata polysaccharides based on response surface methodology and their antioxidant activities. *Carbohydr Polym*. 2016;148:345–353. doi:10.1016/j.carbpol.2016.04.081
17. Meng FD, Yuan L, Lu DD, et al. Anti-tumor effect of coix seed based on the theory of medicinal and food homology. *World J Clin Oncol*. 2023;14(12):593–605. doi:10.5306/wjco.v14.i12.593
18. Sokary S, Al-Asmakh M, Zakaria Z, et al. The therapeutic potential of matcha tea: a critical review on human and animal studies. *Curr Res Food Sci*. 2023;6:100396. doi:10.1016/j.crfs.2022.11.015
19. Wei P, Zhao F, Wang Z, et al. Sesame (Sesamum indicum L.): a comprehensive review of nutritional value, phytochemical composition, health benefits, development of food, and industrial applications. *Nutrients*. 2022;14(19):4079. doi:10.3390/nu14194079
20. Gao Q, Chen N, Li B, et al. Natural lipid nanoparticles extracted from Morus nigra L. leaves for targeted treatment of hepatocellular carcinoma via the oral route. *J Nanobiotechnol*. 2024;22(1):4. doi:10.1186/s12951-023-02286-3
21. Schuh C, Aguayo S, Zavala G, et al. Exosome-like vesicles in Apis mellifera bee pollen, honey and royal jelly contribute to their antibacterial and pro-regenerative activity. *J Exp Biol*. 2019;222(Pt 20). doi:10.1242/jeb.208702.
22. Chen X, Liu B, Li X, et al. Identification of anti-inflammatory vesicle-like nanoparticles in honey. *J Extracell Vesicles*. 2021;10(4):e12069. doi:10.1002/jev2.12069
23. Xiao K, Li H, Li Y, et al. Protective effects and mechanism of Sangyu granule on Acetaminophen-induced liver injury in mice. *J Ethnopharmacol*. 2024;331:118282. doi:10.1016/j.jep.2024.118282

24. Ouyang Y, Virasch N, Hao P, et al. Suppression of human IL-1beta, IL-2, IFN-gamma, and TNF-alpha production by cigarette smoke extracts. *J Allergy Clin Immunol*. 2000;106(2):280–287. doi:10.1067/mai.2000.107751
25. Dong Y, Zhang K, Wei J, et al. Gut microbiota-derived short-chain fatty acids regulate gastrointestinal tumor immunity: a novel therapeutic strategy? *Front Immunol*. 2023;14:1158200. doi:10.3389/fimmu.2023.1158200
26. Pegtel DM, Gould SJ. Exosomes. *Annu Rev Biochem*. 2019;88:487–514. doi:10.1146/annurev-biochem-013118-111902
27. Cong M, Tan S, Li S, et al. Technology insight: plant-derived vesicles-How far from the clinical biotherapeutics and therapeutic drug carriers? *Adv Drug Deliv Rev*. 2022;182:114108. doi:10.1016/j.addr.2021.114108
28. Munagala R, Aqil F, Jeyabalan J, et al. Bovine milk-derived exosomes for drug delivery. *Cancer Lett*. 2016;371(1):48–61. doi:10.1016/j.canlet.2015.10.020
29. Ren J, He W, Zheng L, et al. From structures to functions: insights into exosomes as promising drug delivery vehicles. *Biomater Sci*. 2016;4(6):910–921. doi:10.1039/C5BM00583C
30. Ju S, Mu J, Dokland T, et al. Grape exosome-like nanoparticles induce intestinal stem cells and protect mice from DSS-induced colitis. *Mol Ther*. 2013;21(7):1345–1357. doi:10.1038/mt.2013.64
31. El-Far AH, Tantawy MA, Al Jaouni SK, et al. Thymoquinone-chemotherapeutic combinations: new regimen to combat cancer and cancer stem cells. *Naunyn Schmiedebergs Arch Pharmacol*. 2020;393(9):1581–1598. doi:10.1007/s00210-020-01898-y
32. Shehatta NH, Okda TM, Omran GA, et al. Baicalin; a promising chemopreventive agent, enhances the antitumor effect of 5-FU against breast cancer and inhibits tumor growth and angiogenesis in Ehrlich solid tumor. *Biomed Pharmacother*. 2022;146:112599. doi:10.1016/j.biopha.2021.112599
33. Xu H, Li L, Wang S, et al. Royal jelly acid suppresses hepatocellular carcinoma tumorigenicity by inhibiting H3 histone lactylation at H3K9la and H3K14la sites. *Phytomedicine*. 2023;118:154940. doi:10.1016/j.phymed.2023.154940
34. Roderburg C, Luedde T. The role of the gut microbiome in the development and progression of liver cirrhosis and hepatocellular carcinoma. *Gut Microbes*. 2014;5(4):441–445. doi:10.4161/gmic.29599
35. Behary J, Amorim N, Jiang XT, et al. Gut microbiota impact on the peripheral immune response in non-alcoholic fatty liver disease related hepatocellular carcinoma. *Nat Commun*. 2021;12(1):187. doi:10.1038/s41467-020-20422-7
36. Schwabe RF, Greten TF. Gut microbiome in HCC - Mechanisms, diagnosis and therapy. *J Hepatol*. 2020;72(2):230–238. doi:10.1016/j.jhep.2019.08.016
37. Zhu Y, Chen B, Zhang X, et al. Exploration of the muribaculaceae family in the gut microbiota: diversity, metabolism, and function. *Nutrients*. 2024;16(16):2660. doi:10.3390/nu16162660
38. Pei L, Liu W, Liu L, et al. Morel (Morchella spp.) intake alters gut microbial community and short-chain fatty acid profiles in mice. *Front Nutr*. 2023;10:1237237. doi:10.3389/fnut.2023.1237237
39. Ormerod KL, Wood DL, Lachner N, et al. Genomic characterization of the uncultured Bacteroidales family S24-7 inhabiting the guts of homeothermic animals. *Microbiome*. 2016;4(1):36. doi:10.1186/s40168-016-0181-2
40. Icard P, Simula L, Wu Z, et al. Why may citrate sodium significantly increase the effectiveness of transarterial chemoembolization in hepatocellular carcinoma? *Drug Resist Updat*. 2021;59:100790. doi:10.1016/j.drup.2021.100790
41. Fruman DA, Chiu H, Hopkins BD, et al. The PI3K pathway in human disease. *Cell*. 2017;170(4):605–635. doi:10.1016/j.cell.2017.07.029
42. Liu W, Zheng L, Zhang R, et al. Circ-ZEB1 promotes PIK3CA expression by silencing miR-199a-3p and affects the proliferation and apoptosis of hepatocellular carcinoma. *Mol Cancer*. 2022;21(1):72. doi:10.1186/s12943-022-01529-5
43. Matter MS, Decaens T, Andersen JB, et al. Targeting the mTOR pathway in hepatocellular carcinoma: current state and future trends. *J Hepatol*. 2014;60(4):855–865. doi:10.1016/j.jhep.2013.11.031